# Preparation of a Vast $CoFe_2O_4$ Magnetic Monolayer by Langmuir−Blodgett Technique

**Don Keun Lee,[†] Young Hwan Kim,[†] Young Soo Kang,*[,†] and Pieter Stroeve[‡]**

*Department of Chemistry, Pukyong National University, 599-1 Daeyeon-3-dong, Nam-gu, Pusan 608-737, South Korea, and Department of Chemical Engineering and Materials Science, University of California, Davis, Davis, California 95616*

*Received: May 6, 2005; In Final Form: June 14, 2005*

The preparation of ultrathin films of $CoFe_2O_4$ nanocrystallites is reported. TEM images of them showed 2-dimensional assembly of particles, demonstrating the uniformity of these nanocrystallites. The formation of a Langmuir monolayer of the surface coated $CoFe_2O_4$ nanocrystallites with oleate at the air/water interface and its stability were studied with pressure−area isotherm curves and Brewster Angle Microscope (BAM) images. Surface pressure vs surface area isotherms and TEM studies demonstrated that the increasing surface pressure resulted in a transition from a complex with well-separated domains of nanocrystallites to well-compressed, monoparticulate layers, and, ultimately, to multiparticulate layers.

## Introduction

Novel nanocrystalline properties arise from the large fraction of atoms which reside on the surface of the particles and from the finite number of atoms in each crystalline core. It was in magnetic systems that the first finite size effects were recognized[1] and more subtle effects were later noted in nonmagnetic metals.[1−6] Recently, the development of uniform magnetic nanoparticles of ∼10 nm became a very important issue in their application to ultra-high-density magnetic storage devices[7] and as soft magnetic material of a nanocomposite permanent magnet.[8] Magnetic storage technology is advancing more rapidly toward its scaling limits. Thin granular films of ferromagnetic nanoparticles formed by sputter deposition are already the basis of conventional rigid magnetic storage media hard drives. Progress in magnetic recording density is due in part to the development of media with finer grain magnetic films. The figure of merit by which permanent-magnet materials are judged is the energy product—a measure of the maximum magnetostatic energy that would be stored in free space between the pole pieces of a magnet made from the material in question. About a decade ago, an idea emerged that brought new hope. This is the concept of exchange coupling between a hard magnetic (high-coercivity) material and a soft magnetic (low-coercivity) material with a large magnetization. In a two-phase mixture of such materials, exchange forces between the phases mean the resulting magnetization and coercivity of the material will be some average of the properties of the two constituent phases.[9] But for the exchange coupling to be effective, the relative sizes of the grains of the two materials must be chosen carefully. Typically, this limits the soft phase to grains about 10 nm in diameter. Numerous physical and chemical methods have been employed to produce metal nanocrystals, including sputtering, metal evaporation, grinding, electrodeposition, solution phase metal salt reduction, and neutral organometallic precursor decomposition.[10] Significant progress has been made in preparing nearly monodispersed noble metal nanocrystals of Au, Ag, Pd, and Pt.[11−13]

The most important thing for application is not only the shrinking in size but also the arrangement of nanoparticles. A variety of techniques for the formation of ultrathin films with nanoparticles are available and include spin-coating, self-assembly, sputtering, plasma polymerization, and Langmuir−Blodgett (LB) film deposition.[14,15] But the unmediated self-assembly of monodisperse nanoparticles can only offer limited packing orders with almost no control of the domain structure, packing density, and number of layers deposited. Among the techniques for the deposition of thin films of nanoparticles on solid substrates, layer-by-layer deposition and Langmuir−Blodgett (vertical lift) techniques are some of the most promising methods because they enable fine control of the thickness and homogeneity of the monolayer and ease for multilayer deposition.[16−19] Recently, Werts et al. have shown that it was possible to pattern LB films of gold nanoparticles.[20] Although several methods have been explored in making a monolayer film of nanoparticles, the monolayer on a substrate is typically smaller than 1 $\mu$m × 1 $\mu$m in certain regions. The approach is not ideally suitable for generating a highly ordered and close-packed homogeneous monolayer of nanoparticles, which is potentially important for applications.[21]

In the present study, $CoFe_2O_4$ nanocrystallites were obtained by a very easy, economical, and nontoxic thermal decomposition method and stabilized by coating with oleic acid. We here describe the preparation of ultrathin films of $CoFe_2O_4$ nanocrystallites (in uniform diameter, ca. 9.5 ± 1.3 nm) on a water subphase and their subsequent transfer to solid substrates using the LB technique.

## Experimental Section

**Preparation of $CoFe_2O_4$ Nanocrystallite.** Figure 1 shows a procedure for the synthesis of monodispersed $CoFe_2O_4$ nanocrystallites and the preparation of a Langmuir−Blodgett film of $CoFe_2O_4$ nanocrystallites. $FeCl_2 \cdot 4H_2O$ (99+%), $CoCl_2 \cdot 6H_2O$ (98%), and sodium oleate ($C_{17}H_{33}COONa$, 98%) were obtained from Aldrich Chemical Co. and used without further purification. To prepare the iron−oleate complex, 1.995 g of $FeCl_2 \cdot 4H_2O$ (10 mmol) and 1.190 g of $CoCl_2 \cdot 6H_2O$ (5 mmol) were dissolved in deoxygenated water (300 mL, 18 MΩ,

* Address correspondence to this author. E-mail: yskang@pknu.ac.kr.
† Pukyong National University.
‡ University of California, Davis.

10.1021/jp052363x CCC: $30.25 
Published on Web 07/16/2005

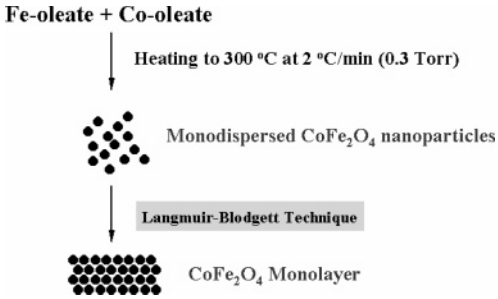


**Figure 1.** Precedure of the synthesis of $CoFe_2O_4$ nanaocrystallites and the preparation of a Langmuir−Blodgett film.

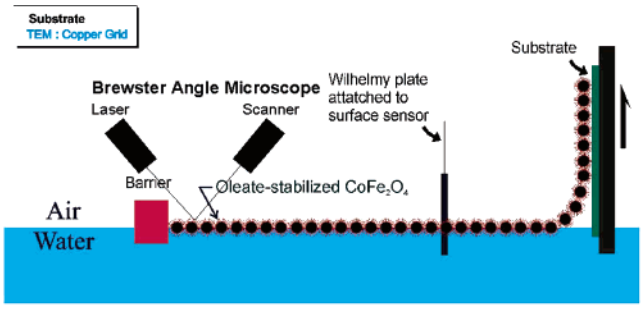


**Figure 2.** Schematic drawing of Langmuir−Blodgett depostion of an oleate-stabilized $CoFe_2$ nanacrystallite monolayer at the air/water interface.

nitrogen gas bubbling for 30 min) and the resulting solution was added into 9.135 g of sodium oleate (30 mmol) under vigorous stirring for 2 h. The precipitate was separated by filtration and doubly washed with deionized water to be free of sodium and chlorine ions. After drying the iron−oleate complex was transferred into the Pyrex tube. The complex was first flushed with nitrogen, and the tube was sealed at 0.3 Torr. The sample was slowly heated from room temperature to 300 °C at 1 °C/min. After reaching the desired temperature, it was held at 300 °C for 2 h and cooled to room temperature. The complex color was changed to black, indicating that $CoFe_2O_4$ nanocrystallites were being formed. These $CoFe_2O_4$ nanocrystallites can be easily redispersed in octane or toluene due to surface coating by oleate. When metal−oleate complexes are decomposed at high temperature, metal ions become metal nanoparticles and oleate ions surround them.

**Preparation of a Langmuir−Blodgett Film of $CoFe_2O_4$ Nanocrystallite.** The pressure−area isotherms of the surface-coated $CoFe_2O_4$ nanocrystallites at the air/water interface were obtained with a KSV minitrough (45 cm × 15 cm, KSV model 2200). Figure 2 shows schematic drawings of the pressure−area isotherm experiment and LB deposition of the surface-coated $CoFe_2O_4$ Langmuir monolayer at the air/water interface. The setup included a surface pressure microbalance with a Wilhelmy plate. The trough system was controlled by a computer and KSV Film Control System Software. Isotherm compression and data collection were automatically achieved through the use of computer software. The Langmuir−Blodgett film of the surface-coated $CoFe_2O_4$ nanoparticle was prepared by transferring the monolayer with use of the Langmuir−Blodgett technique. The trough must be carefully placed to ensure that it was completely leveled and that there was a good seal between trough and barrier; this is essential to the monolayer compression. A stock solution was prepared by dissolving 10 mg of the surface-coated $CoFe_2O_4$ in 10 mL of chloroform. The subphase temperature was controlled with a Jeio Tech Co. Ltd. Refrigerated Circulator, Model RBC 20.

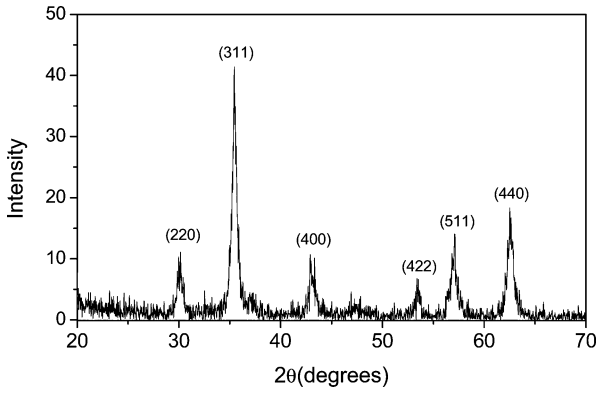


**Figure 3.** X-ray diffraction pattern (Cu Kα radiation) of $CoFe_2O_4$ nanocrystallites.

**Brewster Angle Microscopy Study.** In the experimental setup of the Brewster Angle Microscope (BAM) (NanoFilm Tech., Germany) used for the characterization of monolayers and interfacial processes, the light beam of a pulsed laser ($\lambda$ = 532 nm, beam diameter of 1 mm) passed through a polarizer (set for p-polarization) was incident on the air/water interface at the Brewster angle (53.15°). The reflected beam was detected with a CCD camera. An image of the interface was formed through a microscope coupled to the CCD inclined at the Brewster angle, which collected the reflected light and a part of the light scattered by the interface. BAM images were recorded in situ with the NanoFilm Technology BAM 2 Plus on the KSV 2000 trough.

**Experimental Technique.** To identify properties of the synthesized $CoFe_2O_4$ nanoparticles, we made various experiments. The crystal structure of the synthesized nanoparticles was identified by using X-ray powder diffraction (XRD) with a Philips X'Pert-MPD System with a Cu Kα radiation source ($\lambda$ = 0.154056 nm). The size and shape of nanoparticles were obtained by transmission electron microscopy (TEM). TEM measurements were carried out on a HITACHI H-7500 (low-resolution) and a JEOL JEM2010 (high-resolution) transmission electron microscope. Samples for TEM samples were prepared on 300 mesh copper grids coated with carbon. A drop of $CoFe_2O_4$ nanoparticle solutions was carefully placed on the copper grid surface and dried. The size distributions of the particles were measured from enlarged photographs of the TEM images. Elemental analyses of them conducted by using energy-dispersive X-ray microanalysis (EDX) are carried out on a JEOL JEM2010 TEM operated under an acceleration voltage of 200 kV. The magnetization curves were characterized with a Lake Shore 7300 vibrating sample magnetometer (VSM). The size distribution and the characterization of the nanocomposite film of the surface-coated $CoFe_2O_4$ nanocrystallites were identified with TEM analysis.

## Results and Discussion

**Crystal Structure and Average Size.** Figure 3 illustrates the XRD pattern of the surface-coated $CoFe_2O_4$ nanocrystallite sample. No impurity peak was observed in the XRD pattern. The diffraction peaks were clearly broadened, which could be the result of the reduced particle size. The discernible peaks can be indexed to (220), (311), (400), (422), (511), and (440) planes of a cubic unit cell, which corresponds to that of a $CoFe_2O_3$ structure (JCPDS card no. 22-1086). Figure 4 shows a low-resolution TEM image of $CoFe_2O_4$ nanocrystallites. The $CoFe_2O_4$ nanocrystallite monolayer was formed by self-assembly when a drop of the nanocrystallite isooctane solution

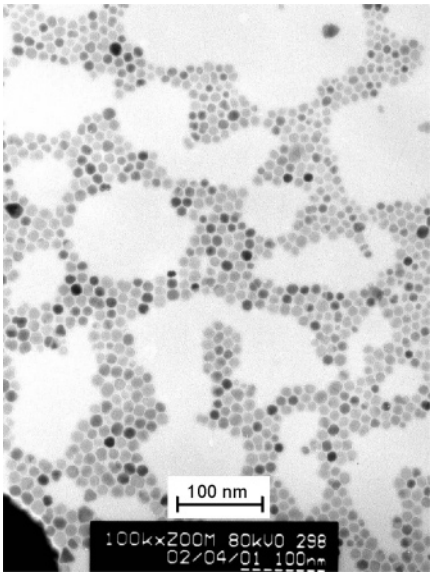


**Figure 4.** TEM image of $CoFe_2O_4$ nanocrystallites.

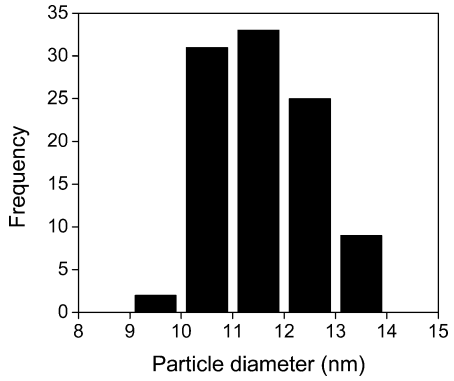


**Figure 5.** Particle size statistics over 150 particles in the TEM micrograph of $CoFe_2O_4$ nanocrystallites.

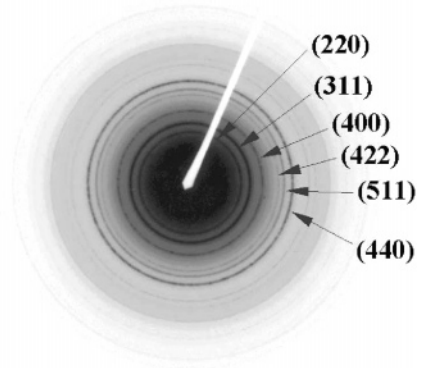


**Figure 6.** ED pattern of $CoFe_2O_4$ nanocrystallites.

was carefully placed on the grid and dried in air. Most of the $CoFe_2O_4$ particles are spherical.

Figure 5 shows the histogram of the size distribution of $CoFe_2O_4$ nanocrystallites obtained from the TEM picture. The mean size of $CoFe_2O_4$ nanocrystallites is 11.1 nm with a standard deviation of 1.5 nm. This shows that the $CoFe_2O_4$ nanocrystallites have very narrow size distribution. Figure 6 shows that the selected area electron diffraction (SAD) pattern exhibits a $CoFe_2O_4$ structure. It revealed dense ring patterns with *d*-spacings of 3.01, 2.54, 2.11, 1.63, and 1.49 Å, which match the standard body centered cubic spinel structure of cobalt iron oxide lines (JCPDS card, no.22-1086). The diffraction rings

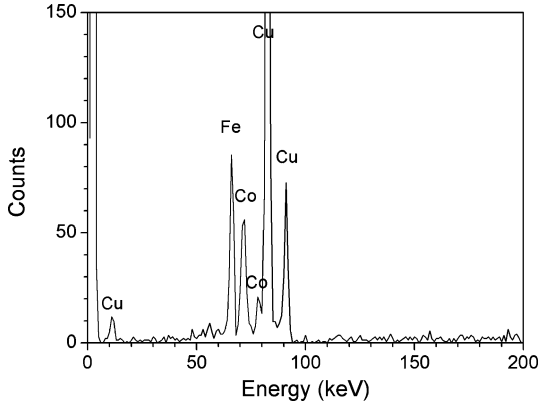


**Figure 7.** Energy-dispersive X-ray spectrum of $CoFe_2O_4$ nanocrystallites.

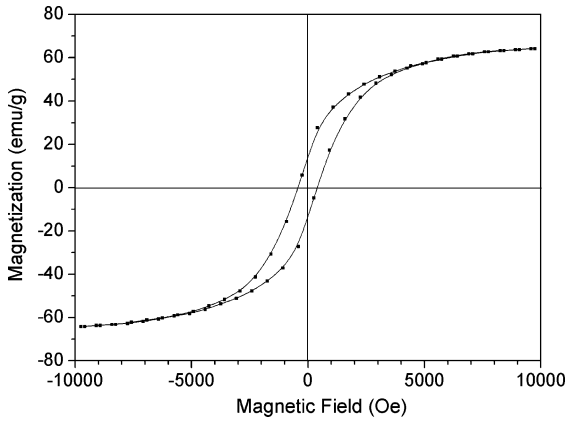


**Figure 8.** Magnetization versus applied field at 300 K for $CoFe_2O_4$ nanocrystallites.

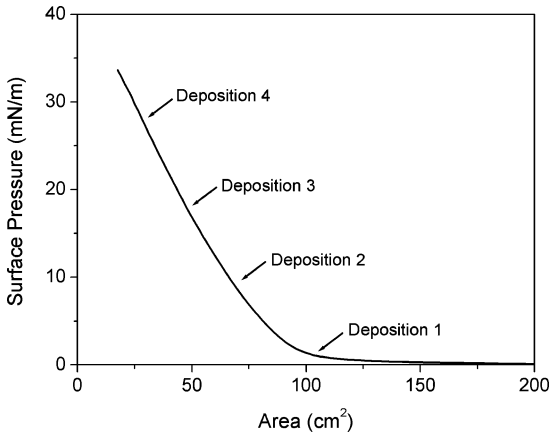


**Figure 9.** The pressure−area isotherm of the surface-coated $CoFe_2O_4$ nanocrystallites at the air/water interface at 25 °C.

can be indexed to (220), (311), (400), (422), (511), and (440) planes at a silver nanocrystallite. The same result is observed for XRD spectra of Figure 3. This indicates that the nanocrystallites in the TEM image are $CoFe_2O_4$.

**Atomic Molar Ratio and Magnetic Property.** Figure 7, showing an EDX spectrum of the surface-coated $CoFe_2O_4$ nanocrystallite, shows that clear peaks of Co and Fe were detected. $CoFe_2O_4$ nanocrystallites indicated the presence of Co and Fe with the atomic ratio of Co:Fe = 1:2.

Figure 8 shows magnetization versus applied field at 300 K for the surface-coated $CoFe_2O_4$ nanoparticles. This demonstrates that the synthesized $CoFe_2O_4$ nanocrystallites are not very hard magnetic material, because of the small coercivity $H_c$ = 460

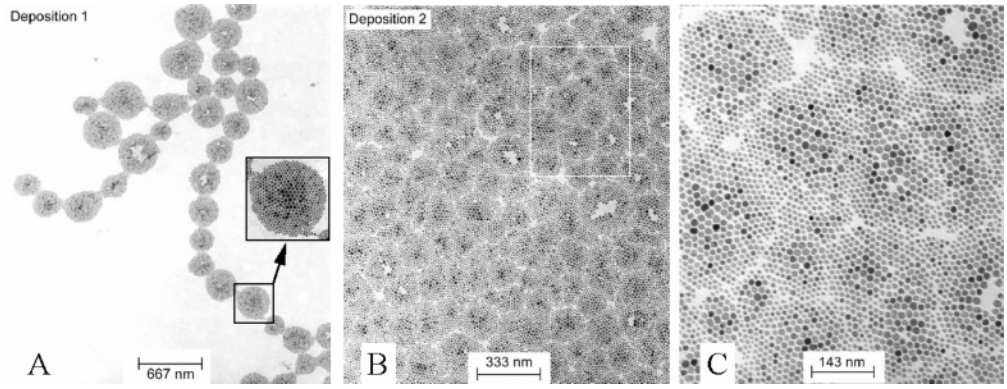


**Figure 10.** TEM images of LB films deposited at different surface pressures of 2 (A) and 8 mN/m (B and C) in the subphase of water at 25 °C.

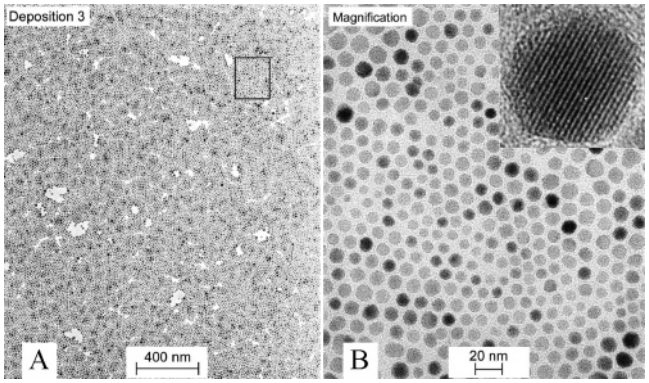


**Figure 11.** TEM images of a LB film deposited at the surface pressure of 17 mN/m in the subphase of water at 25 °C. A monolayer of nanoparticles is observed from the image with almost no any multiplayer on it. (A) Low-magnification TEM image and (B) high-magnification TEM image of a monodispersed nanocrystallite and a lattice image of a single nanocrystallite (inset) of 11 nm $CoFe_2O_4$ nanocrystallite.

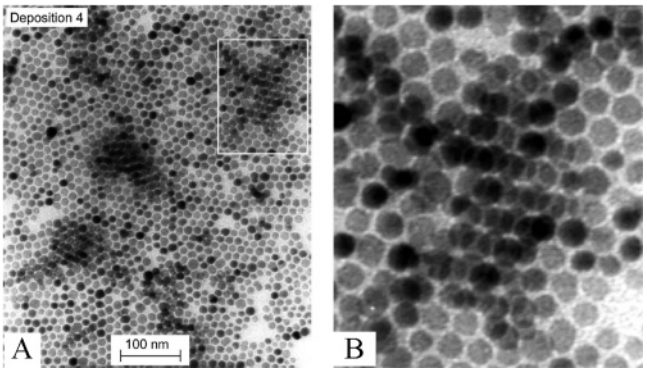


**Figure 12.** TEM image of LB films deposited at the surface pressure of 27 mN/m in the subphase of water at 25 °C (A). Magnified image of a white quadrangle of the left TEM image showing a three-dimensional close-packed superlattice assembly (B).

Oe and high saturation magnetization ($M_s$ = 64.2 emu/g).[22] These values are much smaller than those of the bulk ferrite, 980 Oe. Although the critical size of cobalt ferrite showing superparamagnetic relaxation at room temperature is not theoretically known, it is known that $CoFe_2O_4$ in the size range of 10−30 nm shows no superparamagnetic relaxation up to room temperature. It can be inferred that the critical size of $CoFe_2O_4$ for superparamagnetic relaxation at room temperature lies roughly between 4 and 9 nm. Our $CoFe_2O_4$ nanoparticle (about 11.1 nm) does not have a superparamagnetic property. Comparing with superparamagnetic $Fe_3O_4$ nanoparticle, the $CoFe_2O_4$ nanoparticle has larger coercivity at room temperature.

**The Study of Langmuir Monolayer and TEM Images.** Molecules in a solution are subject to attractive forces; in the bulk of the solution these forces are equal. However, at a surface or interface the forces are unequal and the net effect is to pull the peripheral molecules into the bulk of the solution. This effect gives rise to surface tension. The surface tension can be defined as the work required to expand the surface isothermally by unit area. The tendency of surface-active molecules to accumulate at interfaces favors expansion of the interface and hence lowers the surface tension. Such behavior makes it possible to monitor the surface pressure as a function of the area occupied per molecule provided that the number of molecules deposited on the surface is known. Figure 9 shows the pressure−area isotherm of the surface-coated $CoFe_2O_4$ nanocrystallites at the air/water interface. This demonstrates a successful formation of a Langmuir monolayer of the surface-coated $CoFe_2O_4$. As the area is reduced, at first there is a coexistence between the gas and the liquid crystalline phases at very low surface pressures. The isotherm curves then do not show a typical continuous transition from a liquid tilted crystalline phase to an untilted phase.[23,24] It seems that soft oleic acid molecules between $CoFe_2O_4$ nanocrystallites in the Langmuir monolayer at the air/water interface prevent phase transition from the liquid phase to the solid phase. Samples for TEM measurement were prepared at different surface pressures of 2 (Deposition 1), 8 (Deposition 2), 17 (Deposition 3), and 27 mN/m (Deposition 4) by the LB technique.

Figure 10 shows TEM images of LB films deposited at surface pressures of 2 (A) and 8 mN/m (B and C) in the pure water subphase at 25 °C. In Figure 10A, ian slandlike monolayer was formed at the air/water interface. This is due to hydrophobic interaction between the hydrophobic surface-coated nanoparticles as if a hydrophobic oil was spread on water. As shown the inset of Figure 10A, the cluster is perfectly monolayer. But these images demonstrate that $CoFe_2O_3$ nanocrystallites do not form a long-range ordered monolayer at surface pressures of 2 and 8 mN/m.

Figure 11A shows low-magnification TEM images of LB films deposited at a surface pressure of 17 mN/m in the pure water subphase at 25 °C. A monolayer of nanocrystallite was observed from the image with almost no double layers or multilayers in it. It shows an example of an extended area where particles are packed in a highly organized manner, exhibiting a remarkable degree of long-range order. The size of the TEM photograph is 2 $\mu$m × 2.6 $\mu$m. Figure 11B shows a high-magnification TEM image of the LB film and a high-resolution TEM image of a single $CoFe_2O_4$ nanocrystallite (inset). It demonstrates that monodispersed $CoFe_2O_4$ nanocrystallites were arranged in a 2-dimensional hexagonal closed packed way, demonstrating the uniformity of the particle size. Especially the

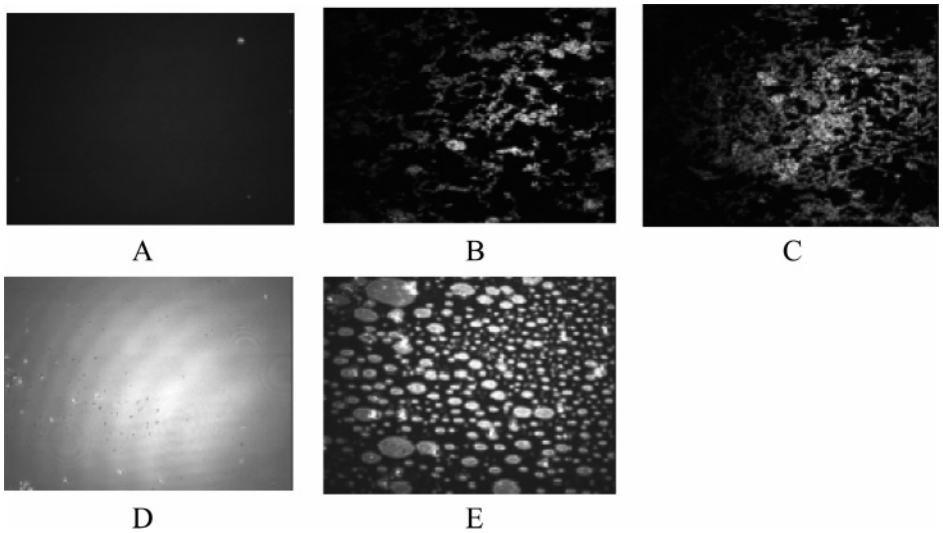


**Figure 13.** BAM images of the $CoFe_2O_4$ nanacrystallite coated by oleate at the air/water interface measured at different surface pressures: 0 (A), 2 (B), 12 (C), 17 (D), and 27 mN/m (E).

interparticle spacing is very even. Here, as in most cases, adjacent $CoFe_2O_4$ nanocrystallites were separated by a region of approximately 2 nm that did not exhibit any diffraction contrast. This distance is considerably less than twice the expected oleate length (1.75 nm);[16] interdigitation of the alkyl chains from nearest-neighbor $CoFe_2O_4$ particles can be inferred. The high-resolution TEM image indicates that the $CoFe_2O_4$ single domain was perfectly synthesized bythe thermal decomposition method without any defect.

Figure 12 shows TEM images of LB films deposited at a surface pressure of 27 mN/m in the pure water subphase at 25 °C (A) and the magnified image of a white quadrangle of the left TEM image (B). These images demonstrate that multilayer of $CoFe_2O_4$ appear. It indicates that the LB monolayer of $CoFe_2O_4$ nanocrystallites was collapsed at a surface pressure of 27 mN/m. Brewster Angle Microscope (BAM) has come into widespread use for the study of monolayers both on liquid and on solid surfaces. BAM is a microscopy technique based upon the characteristics of the reflection of the light at the Brewster angle. The interface to be studied is illuminated by a polarized parallel laser beam in the plane of incidence. The incidence angle is the Brewster angle, which implies that no light is reflected if there is no interfacial layer and no roughness at the interface. The refractive index changes abruptly from the refractive index of one medium to that of the second medium at the level of the interface. Such changes depend strongly on the interfacial properties such as the molecular density and the orientation in the interfacial layer. In this way, an image of the interface can be formed through a microscope inclined at the Brewster angle, which collects the reflected light and a part of the light scattering by the interface.

The phase behavior of the $CoFe_2O_4$ nanocrystallites coated by oleate at the air/water interface was observed with BAM at different pressures, as shown in Figure 13. Figure 13A shows an image of an uncompressed film. Some domains such as those shown in parts B and C of Figure 13 have been observed in simple surfactant monolayers. They have, for example, been viewed by BAM in monolayers formed from stearic acid,[25] pentadecanoic acid,[25,26] and myristic acid.[27] In the case of pentadecanoic acid, bright circles of the liquid crystalline phase in a dark background were observed at a compression corresponding to the liquid expanded/liquid compressed (LE/LC) phase transition. Images of monolayers of myristic acid in the liquid−gas coexistence region comprised dark circles in a bright background and in the LE/LC region, bright circles in a dark background.[27] Interpretation of the images of a monolayer of $CoFe_2O_4$ nanocrystallites coated by oleate is complicated by the existence of the two components. The contrast in the images may derive from the phase structure of an entirely uniform film or from an area rich in either $CoFe_2O_4$ nanocrystallite or oleate. The area of closely packed $CoFe_2O_4$ nanocrystallite will necessarily reflect the incident light more strongly than areas of oleate and this appears brighter. Compression to the surface pressure of 17 mN/m produced a very uniform, dense film (Figure 13D). Figure 13E shows the collapse of the Langmuir monolayer of $CoFe_2O_4$ nanocrystallite at a surface pressure of 27 mN/m.

## Conclusions

A very simple synthetic method has been discovered to produce monodispersed $CoFe_2O_4$ nanocrystallites using thermal decomposition ($9.5 \pm 1.3$ nm). TEM micrographs show that the LB monolayers of $CoFe_2O_4$ nanocrystallites are fabricated in a highly organized manner, exhibiting a remarkable degree of long-range order ($2\ \mu m \times 2.6\ \mu m$).

**Acknowledgment.** This work was supported by the Korean National Laboratory Program. D.K.L. would like to thank financial support by Brain Busan 21.

## References and Notes

(1) Dormann, J. L.; Fiorani, D., Eds. *Magnetic Properties of Fine Particles*; North-Holland: Amsterdam, The Netherlands, 1992.
(2) Perenboom, J.; Wyder, P.; Meier, F. *Phys. Rep.* **1981**, *78*, 173.
(3) Bradley, J. S. In *Cluster and Colloids*; Schmid,G., Ed.; VCH: New York, 1994; p 523.
(4) Klingelhöfer, S.; Heitz, W.; Greiner, A.; Oestreich, S.; Förster, S.; Antonietti, M. *J. Am. Chem. Soc.* **1997**, *119*, 10116.
(5) Bar-Sadeh, E.; Goldstein, Y.; Zhang, C.; Deng, H.; Abeles, B.; Millo, O. *Phys. Rev. B* **1994**, *50*, 8961.
(6) Janes, D. B.; Kolagunta, V. R.; Osifchin, R. G.; Bielefeld, J. D.; Andres, R. P.; Henderson, J. I.; Kubiak, C. P. *Superlattices Microstruct.* **1995**, *18*, 275.
(7) (a) Sun, S.; Murray, C. B.; Weller, D.; Folks, L.; Moser, A. *Science* **2000**, *287*, 1989. (b) Sun, S.; Murray, C. B. *J. Appl. Phys.* **1999**, *85*, 4325.
(8) Zeng, H.; Li, J.; Liu, J. P.; Wang, Z. L.; Sun, S. *Nature* **2002**, *420*, 395
(9) Skomski, R.; Coey, J. M. D. *Phys. Rev. B* **1993**, *48*, 15812.
(10) (a) Petit, C.; Taleb, A.; Pileni, M. P. *J. Phys. Chem. B* **1999**, *103*, 1805. (b) Smith, T. W.; Wychick, D. *J. Phys. Chem.* **1980**, *84*, 1621.
(11) Murray, C. B.; Norris, D. J.; Bawendi, M. G. *J. Am. Chem. Soc.* **1993**, *115*, 8706.
(12) Alivisatos, A. P. *Science* **1996**, *271*, 933.

(13) Rondaninone, A. J.; Samia, A. C. S.; Zhang, Z. J. *J. Phys. Chem. B* **1999**, *103*, 6876.
(14) Kang, Y. S.; Lee, D. K.; Lee, C. S.; Stroeve, P. *J. Phys. Chem. B* **2002**, *106*, 9341.
(15) Kang, Y. S.; Lee, D. K.; Lee, C. S.; Stroeve, P. *J. Phys. Chem. B* **2002**, *106*, 7267.
(16) Stine, K. J.; Moore, B. G. In *Nano-Surface Chemistry*, 1st ed.; Rosoff, M., Ed.; Marcel Dekker: New York, 2001; pp 59−140.
(17) Decher, G. *Science* **1997**, *277*, 1232−1237.
(18) Chen, S. W. *Langmuir* **2001**, *17*, 2878−2884.
(19) Sastry, M.; Mayya, K. S.; Patil, V.; Paranjape, D. V.; Hegde, S. G. *J. Phys. Chem. B* **1997**, *101*, 4954−4958.
(20) Werts, M. H. V.; Lambert, M.; Bourgoin, J.-P.; Brust, M. *Nano Lett.* **2002**, *2*, 43.
(21) Ao, B.; Kummerl, L.; Haarer, D. *Adv. Mater.* **1995**, *7*, 496.
(22) Vicente, J.; Delgado, V.; Plaza, C.; Duran, J. D. G.; Caballero, F. *Langmuir* **2000**, *16*, 7954.
(23) Kaganer, V. M.; Peterson, I. R.; Kenn, R. M.; Shih, M. C.; Durbin, M.; Dutta, P. *J. Chem. Phys.* **1995**, *102*, 9412.
(24) Dutta, P.; Peng, J. B.; Lin, B.; Ketterson, J. B.; Georgopoulos, P.; Ehrlich, S. *Phys. Rev. Lett.* **1987**, *58*, 2228.
(25) Honig D.; Mbbius, D. *Thin Solid Films* **1992**, *210*/*211*, 64.
(26) Honig, D.; Overbeck, G. A.; Mbbius, D. *Adv. Mater.* **1992**, *4a*.
(27) Henon, S.; Meunier, J. *Reo. Sci. Instrum.*, **1991**, *62* (4), 936.